Oxygen-induced reconstruction of Re(10$\bar{1}$0) studied by density functional theory

Payam Kaghazchi and Timo Jacob[*]

University of Ulm, Albert-Einstein-Allee 47, D-89081 Ulm, Germany
(Received 26 September 2009; revised manuscript received 2 January 2010; published 23 February 2010)

Using density functional theory in combination with the *ab initio* atomistic thermodynamics approach, we studied the structure and stability of Re(10$\bar{1}$0) surfaces in contact with an oxygen atmosphere. The calculations indicate that without adsorption of oxygen, the surface is unreconstructed, but adsorption of more than 2 geometrical monolayers causes a (1×3) reconstruction, resembling a surface being composed of {10$\bar{1}$1} microfacets. This structure is able to rationalize the different experimental observations obtained on Re(10$\bar{1}$0) and will be of relevance for catalytic reactions under oxygen-rich conditions.

I. INTRODUCTION

Rhenium has mainly been used in the aircraft industry and as catalyst for petroleum processing.[1] However, since recent years, Re and Re-based catalysts have received much attention due to their high reactivity in many important catalytic reactions such as the selective reduction of NO$_x$ with NH$_3$, the selective oxidation of methanol, thiophene, and hydrodesulfurization, or the ammonia synthesis.[2–7] Besides their catalytic properties certain oxygen-covered Re surfaces were also used to grow Co nanoclusters, thus providing a basis for synthesizing active model catalysts with high selectivity.[8,9]

Before studying catalytic reactions, however, a detailed understanding of the surface structure as well as changes introduced by the adsorption of reactants is indispensable. Due to its relevance for many reactions (e.g., CO oxidation), here, we will focus on the adsorption of atomic oxygen that is known to strongly interact with various transition metals. Consequently, oxygen is capable to modify the surface morphologies or even to form metal oxides.[10,11]

Despite the structural similarities between hcp(10$\bar{1}$0) and fcc(110) surfaces, much less attention has been paid to the former ones. On Re(10$\bar{1}$0) only very few experimental studies have been performed.[12–15] Davis and Rosenthal *et al.* used low-energy electron diffraction (LEED) to investigate the surface morphology of clean Re(10$\bar{1}$0). They found that the clean surface shows an unreconstructed structure exhibiting a (1×1) periodicity,[12,13] which is in line with the behavior observed on (10$\bar{1}$0) surfaces of other 3*d* and 4*d* hcp metals.[11,16] Also using LEED, Zehner *et al.*[14] found the existence of (10$\bar{1}$1) facets after exposing the surface to oxygen at pressures of 1.3×10^{-7} atm or higher and a temperature of $T \sim 888$ K. By heating to 1298 K these facets disappeared and a (1×3)-O overlayer formed on the initial (10$\bar{1}$0) surface. Whether this resembled the periodicity of the surface structure or of an oxygen adlayer remained unclear.

Later, Lenz *et al.*[15] could observe the formation of a (1×3)-2O structure for exposures higher than 4 L at $p < 10^{-13}$ atm. They additionally reported a variety of oxygen overlayers at lower exposures: (2×3)-O for 0.3 L, c(2×4)-2O for 0.7 L, (1×5)-2O for 3.2 L, and (1×4)-2O for an exposure of 3.7 L. These overlayers were prepared by annealing the O/Re(10$\bar{1}$0) system to 520 K < T < 650 K. In contrast to the observations by Zehner *et al.*, they did not find evidence for the formation of facets.

Although experiments agree on the appearance of a (1×3) periodicity, there is still no consensus neither on its nature nor on the coverage of adsorbed oxygen. While on the basis of the obtained LEED patterns and measured changes in the work functions Zehner *et al.* assumed a (1×3)-O structure, Lenz *et al.* proposed a (1×3)-2O configuration (and others) from LEED and angle-resolved ultraviolet photoemission spectroscopy (ARUPS) data. For all structures they assumed that this periodicity was induced by oxygen atoms and not by a reconstruction of the underlying substrate.

In order to better understand the nature of the experimentally observed structures we investigated the oxygen adsorption on unreconstructed and different reconstructed Re(10$\bar{1}$0) surfaces. For this purpose the stability of clean and oxygen-covered surfaces were evaluated by means of density functional theory (DFT) in conjunction with the *ab initio* atomistic thermodynamics approach. In Sec. II, we will briefly describe the DFT calculations and the *ab initio* atomistic thermodynamics method as used in the present work. Our results for bulk Re as well as for the clean and oxygen-covered surfaces of unreconstructed and reconstructed Re(10$\bar{1}$0) are described in Sec. III, allowing us to draw the corresponding surface phase diagram (Sec. III D). Finally, conclusions will be given in Sec. IV.

II. METHOD

In this work, density functional theory is used in conjunction with the *ab initio* atomistic thermodynamics approach[17–20] to evaluate the (p, T)-dependent surface free energies from first principles.

A. DFT calculations

DFT energies for different oxygen overlayers on the surfaces were evaluated using the CASTEP code[21] with Vanderbilt-type ultrasoft pseudopotentials (PPs) (Ref. 22)

and the generalized gradient approximation (GGA) exchange-correlation functional proposed by Perdew, Burke, and Ernzerhof (PBE).[23] Using the local density approximation (LDA) we additionally calculated the stability of the most stable phases (determined with GGA-PBE) and obtained the corresponding phase diagram.

A plane-wave basis set with an energy cutoff of 380 eV was used for all surfaces. The Brillouin zones of the (1×1)-surface unit cells of Re($10\bar{1}0$)-(1×1), -(1×2), -(1×3), and Re($10\bar{1}1$)-(1×1) were sampled with (5×8), (3×8), (2×8), and (4×8) Monkhorst-Pack (MP) **k**-point meshes, respectively. Re($10\bar{1}0$) and Re($10\bar{1}1$) surfaces were modeled with 11-layer and 14-layer slabs, respectively, separated by at least 13 Å vacuum. For each system, the bottom four layers were fixed at the calculated bulk-crystal structure, and the remaining Re atoms and the adsorbates were allowed to freely relax. We thoroughly checked the calculational uncertainties related to pseudopotentials, plane-wave cutoff, **k**-point mesh, slab thickness, and vacuum size (see Appendix) and found an overall numerical uncertainty in relative surface free energies of <8 meV/Å^2 when using the above mentioned parameters.

B. Thermodynamic considerations

DFT in principle is a zero-temperature and zero-pressure technique and cannot be used to study the influence of temperature and pressure on surface properties in the macroscopic regime. But when combined with thermodynamic considerations it becomes an applicable tool for predicting surface properties under realistic environmental conditions at a specific temperature and pressure. Here, we discuss the thermodynamic considerations, which can be used to construct surface phase diagrams for O/Re($10\bar{1}0$).

The most stable surface structure under given conditions (temperature and pressure) is the one with the lowest surface free energy,[20]

$$\gamma(T,\{p_i\},\{N_i\}) = \frac{1}{A}\left[G^{\text{surf}}(T,\{p_i\},\{N_i\}) - \sum_i N_i\mu_i(T,p_i)\right], \quad (1)$$

where G^{surf} is the Gibbs energy of the surface (here slab) containing N_i atoms/molecules of the ith species with the chemical potential $\mu_i(T,p_i)$ of the corresponding reservoir. In the present work, the Re($10\bar{1}0$) surface is considered to be in thermodynamic equilibrium with two reservoirs: Re bulk and an O_2 atmosphere. Therefore, assuming the temperature and pressure dependence of all solid phases to be small, Eq. (1) becomes

$$\gamma(T,p_{O_2},N_{\text{Re}},N_O) = \frac{1}{A}[G^{\text{surf}}(T,p_{O_2},N_{\text{Re}},N_O) - N_{\text{Re}}\mu_{\text{Re}}^{\text{bulk}}$$
$$- N_O\mu_O(T,p_{O_2})]. \quad (2)$$

If we consider the adsorbed oxygen to be in equilibrium with the surrounding O_2 gas phase, the oxygen chemical potential can be expressed as

$$\mu_O(T,p_{O_2}) = \frac{1}{2}\left[E_{O_2}^{\text{tot}} + \bar{\mu}_{O_2}(T,p^0) + k_BT \ln\left(\frac{p_{O_2}}{p^0}\right)\right]. \quad (3)$$

Here, $E_{O_2}^{\text{tot}}$ is the calculated total energy of an isolated O_2 molecule and $\bar{\mu}_{O_2}(T,p^0)$ is the standard chemical potential at temperature T, which includes all the contributions from vibrations and rotations of the molecule, and the ideal gas entropy at 1 atm. Although the standard chemical potentials can be calculated from first principles, for the phase diagram, which will be discussed later, we used the corresponding $\bar{\mu}_{O_2}(T,p^0)$ values from the JANAF thermodynamic tables.[24]

The Gibbs energies of solid phases can be written as

$$G = E_{\text{tot}} + F_{\text{conf}} + F_{\text{vib}} + pV, \quad (4)$$

where E_{tot} is the total electronic energy, F_{conf} is the configurational free energy, and F_{vib} is the vibrational free energy. The largest contribution to Eq. (4) arises from the first term E_{tot}, which in the present work is obtained by DFT calculations. An exact evaluation of F_{conf} needs large computational effort since a huge number of possible configurations of adatoms and substrate must be studied for a given structure. This approach seems to be impractical for open surfaces, which have been studied here, with large number of possible adsorbate sites. Fortunately, for sufficiently low temperatures this term is usually much smaller than the total energy term in Eq. (4) and is almost negligible.

For the most stable configurations obtained from our calculations the vibrational contributions to γ were estimated by

$$\gamma^{\text{vib}}(T) \sim \frac{1}{A}\left[\sum_i^{N_O} F_i^{\text{vib}}(T,\bar{\omega}_i^{\text{surf}}) - \frac{N_O}{2}F^{\text{vib}}(T,\bar{\omega}_{O_2}^{\text{gas}})\right], \quad (5)$$

with

$$F^{\text{vib}}(T,\omega) = \frac{1}{2}\hbar\omega + k_BT \ln(1 - e^{-\hbar\omega/k_BT}), \quad (6)$$

where $\bar{\omega}_i^{\text{surf}}$ is the O-surface stretch frequency of the ith adsorbed oxygen in the corresponding adlayer configuration and $\bar{\omega}_{O_2}^{\text{gas}}$ for the O_2 molecule in the gas phase. It was found that these contributions are rather small and they cause no modifications in the ordering of surface phases. For temperatures below 1300 K this would lead to a maximum temperature shift of <50 K in the surface phase diagram. Therefore, in the present work vibrational contributions have not been included.

Lastly, a rather simple dimensional analysis shows that the last term of Eq. (4), pV term, will be less than $\sim$0.001 meV/Å^2 for pressures up to 1 atm and can therefore also be neglected.

Based on these considerations, we can conclude that the chemical potential of the gaseous phases (here O_2) will dominate the T and p dependence of the surface free energies [see Eq. (2)]. Therefore, when considering differences the Gibbs energies of the slab and the Re bulk can be replaced by their corresponding DFT energies, finally leading to an approximate expression for the surface free energy of

TABLE I. Calculated lattice parameters (a_0 and c_0), bulk modulus (B_0), and cohesive energy (E_{coh}) of bulk Re, determined with USPP and AE approaches using the PBE and LDA exchange-correlation functionals. In addition, the experimental values are given.

Method	a_0 (Å)	c_0 (Å)	B_0 (Mbar)	E_{coh} (eV)
USPP (PBE)	2.78	4.48	3.65	−7.63
USPP (LDA)	2.73	4.41	4.05	−9.45
AE (PBE)	2.78	4.48	3.63	−7.70
AE (LDA)	2.74	4.42	4.06	−9.59
Experiment[a]	2.76[b]	4.46[b]	3.72[b]	−8.03[c]

[a]Reference 25.

[b]At room temperature.

[c]At 0 K and 1 atm.

$$\gamma(T, p_{O_2}) \approx \frac{1}{A}[E_{\text{slab}}^{\text{DFT}} - N_{\text{Re}}g_{\text{Re}}^{\text{bulk}} - N_O\mu_O(T, p_{O_2})], \quad (7)$$

where now $E_{\text{slab}}^{\text{DFT}}$ is the calculated total energy of the (oxygen-covered) surfaces and $g_{\text{Re}}^{\text{bulk}}$ the Gibbs energy of Re bulk.

III. RESULTS AND DISCUSSION

A. Bulk Rhenium

Rhenium is a $5d$ transition metal of group VII, and its melting point of 3180 °C is the third highest among all elements.[25] The equilibrium crystal structure of Rhenium is *hcp*.

Before investigating the corresponding surfaces, the equilibrium lattice constants (a_0 and c_0), the bulk modulus (B_0), as well as the cohesive energy $E_{\text{coh}}(a_0, c_0)$ of Re bulk were determined with the PBE and LDA functionals. The results are given in Table I together with the experimental values for comparison. For checking the accuracy of the used Re pseudopotential, these quantities were also calculated with a full-potential all-electron (AE) approach using the WIEN2K code.[26] Comparison between AE and ultrasoft pseudopotential (USPP) results shows no significant difference in the calculated Re bulk properties considering both PBE and LDA.

The PBE lattice constants of a_0 and c_0 calculated with the pseudopotential approach are about 0.7 and 0.5% larger than the experimental values, while LDA underestimates these parameters by 1.1%. The calculated bulk modulus is only 1.9% lower than the experimental value when using the PBE functional, but 8.9% larger based on LDA. Therefore, similar to the DFT-GGA results for other transition metals such as Ag, Pd, Rh, or Cu,[27–30] there is a slight overestimation of a_0 and an underestimation of B_0 compared to the corresponding experimental values. Furthermore, the cohesive energy determined by USPP-PBE is significantly smaller (1.82 eV) than the LDA value and much better compares to the experimental value.
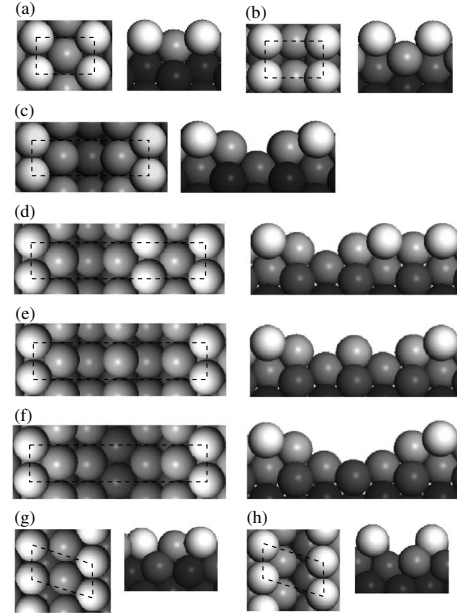
FIG. 1. Top and side views of (a) Re($10\bar{1}0$)A-(1×1), (b) Re($10\bar{1}0$)B-(1×1), (c) Re($10\bar{1}0$)-(1×2) MR, (d) Re($10\bar{1}0$)-(1×3) single MR, (e) Re($10\bar{1}0$)-(1×3) double MR, (f) Re($10\bar{1}0$)-(1×3) triple MR, (g) Re($10\bar{1}1$)A-(1×1), and (h) Re($10\bar{1}1$)B-(1×1) surfaces.

B. Clean Re surfaces

For hcp crystals most surface orientations have two different possible stacking arrangements. Regarding Re($10\bar{1}0$) and Re($10\bar{1}1$), which are the surfaces of interest in the present work, both terminations are distinguished by labels A and B. On the basis of the calculated lattice constants the following surfaces have been considered (see Fig. 1):

(i) unreconstructed Re($10\bar{1}0$) [Figs. 1(a) and 1(b)];

(ii) reconstructed Re($10\bar{1}0$) [Figs. 1(c)–1(f)]; and

(iii) Re($10\bar{1}1$) [Figs. 1(g) and 1(h)], which corresponds to the faces of the facets that experimentally have been observed on Re($10\bar{1}0$).

Among the reconstructed Re($10\bar{1}0$) surfaces we concentrated on (1×2) and different (1×3) reconstructions. While the former periodicity has been observed on several $5d$ fcc(110) metals,[31–37] the (1×3) structures were motivated by the experimental observations.[14,15] The following Re($10\bar{1}0$)-(1×3) reconstructions have been studied [Figs. 1(d)–1(f)]:

(i) single-MR (missing row), where every third top-layer row had been removed (along the $[1\bar{2}10]$ direction);

(ii) double-MR, where every second and third top-layer rows had been removed; and

(iii) triple-MR, where additionally the second-layer row in the center of each trough had been removed. Interestingly, structure (iii) can be viewed as $\{10\bar{1}1\}$ microfacets on the ($10\bar{1}0$) surface.

The calculated surface free energies for the clean surfaces are listed in Table II. We find that, among the studied sur-

TABLE II. Surface free energies (in meV/Å^2) for different clean planar Re(10$\bar{1}$0) and Re(10$\bar{1}$1) surfaces, as well as (10$\bar{1}$1) facets (see Ref. 38 for details).

Structure	γ	Structure	γ
Re(10$\bar{1}$0)A	183	Re(10$\bar{1}$1)A	213
Re(10$\bar{1}$0)B	251	Re(10$\bar{1}$1)B	243
Re(10$\bar{1}$0)A-(1×2) MR	236	Re(1011)A facets	250
Re(10$\bar{1}$0)A-(1×3) single-MR	216		
Re(10$\bar{1}$0)A-(1×3) double-MR	240		
Re(10$\bar{1}$0)A-(1×3) triple-MR	221		

faces, unreconstructed Re(10$\bar{1}$0)A is most stable with a surface free energy of 183 meV/Å^2. As expected, the alternative surface termination Re(10$\bar{1}$0)B, whose surface is less densely packed, has a 68 meV/Å^2 lower stability. The higher stability of Re(10$\bar{1}$0)A is accompanied with a relatively large inward relaxation of the first surface layer by −16.1% compared to the bulk-truncated geometry, which is in good agreement with the LEED-experiments by Davis *et al.*, giving a value of −17%.[12] They also proposed an expansion between the second and third layers by 1%–2% for which we find an insignificant contraction of 0.1%. In comparison, the stabilities of all reconstructed surfaces fit between the values of Re(10$\bar{1}$0)A and Re(10$\bar{1}$0)B, with a certain preference for symmetric surface structures. For instance, Re(10$\bar{1}$0)-(1×3) single MR and triple MR have similar stabilities, which are both lower than the γ value of Re(10$\bar{1}$0)-(1×3) double-MR. Overall our calculations indicate no surface reconstruction for clean Re(10$\bar{1}$0), which is also in line with the experimental observations of Davis *et al.*[12] Since after adsorption of oxygen Zehner *et al.* observed {10$\bar{1}$1} facets on Re(10$\bar{1}$0), we also evaluated the stability of Re(10$\bar{1}$0) fully covered by {10$\bar{1}$1} facets, but found this surface to be thermodynamically unfavorable (see Ref. 38 for details).

C. Oxygen adsorption on Re surfaces

After the clean surfaces, the adsorption of atomic oxygen has been studied on the different surfaces assuming various coverages θ:

(i) Re(10$\bar{1}$0)-(1×1): 0.25, 0.33, 0.50, 0.66, 1.00, 1.33, 1.66, and 2.00 GML;

(ii) Re(10$\bar{1}$0)-(1×2): 0.50, 1.00, 1.50, 2.00 GML;

(iii) Re(10$\bar{1}$0)-(1×3): 0.33, 0.66, 1.00, 1.33, 1.66, and 2.00 GML; and

(iv) Re(10$\bar{1}$1)-(1×1): 0.25, 0.50, 1.00, and 2.00 GML.

Here, we used geometrical coverages [geometrical monolayers (GMLs)], which are defined as the number of adsorbed O atoms per corresponding (1×1)-unit cell (dashed boxes in Fig. 1). For systems with more than one adsorbate per unit cell, several combinations of adsorption sites have
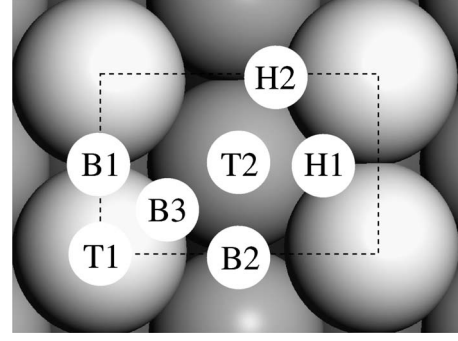
FIG. 2. Top view of Re(10$\bar{1}$0) showing all binding sites at which O adsorption has been studied.

been studied. These configurations have been chosen by considering the calculated energies for lower coverages, and then trying to find the lowest destabilization due to adsorbate-adsorbate repulsion at higher coverages. All structures studied in this work are relaxed with no surface symmetry constraints in order to find the lowest energy configuration.

The most stable structure at a given coverage is the one with the largest average binding energy as defined by

$$\bar{E}_{\text{bind}} = -\frac{1}{N_O}\left[E_{\text{O/Re-slab}} - E_{\text{Re-slab}} - N_O\left(\frac{1}{2}E_{\text{O}_2}\right)\right], \quad (8)$$

where N_O is the number of oxygen atoms in the considered unit cell, $E_{\text{O/Re-slab}}$, $E_{\text{Re-slab}}$, and E_{O_2} are the total energies of the oxygen-covered Re surface, the clean Re surface, and an isolated oxygen molecule. According to this definition a positive number indicates that the dissociative adsorption of oxygen from gas-phase O$_2$ is exothermic.

1. Unreconstructed O/Re(10$\bar{1}$0)-(1×1)

In order to determine the preferred oxygen binding sites on unreconstructed Re(10$\bar{1}$0)-(1×1), we first considered one adsorbate per unit cell. Figure 2 shows several different binding sites at which oxygen binding has been studied. Independent of the coverage oxygen prefers the threefold H1 site, where adatoms are bound to two top Re atoms and one Re atom in the second layer. This adsorption site was also found for O on Co(10$\bar{1}$0) by LEED analysis[16] or on Ru(10$\bar{1}$0) by DFT calculations.[11] Focusing on oxygen at H1 sites, Fig. 3 shows the various overlayers considered for different coverages, while the corresponding binding energies are summarized in Table III.

The lowest coverage structures that have been studied are the (2×2)-1O and c(2×4)-1O overlayers with 0.25 GML shown in Figs. 3(a1) and 3(a2). Due to the rather large O-O separation and the weak lateral adatom interactions, the corresponding binding energies of 3.76 and 3.75 eV, respectively, (almost) represent the behavior for the zero coverage limit.

For the slightly increased coverage of 0.33 GML we have evaluated the (1×3)-1O [Fig. 3(b1)] and (3×1)-1O overlayers [Fig. 3(b2)]. It turned out that the latter configuration,
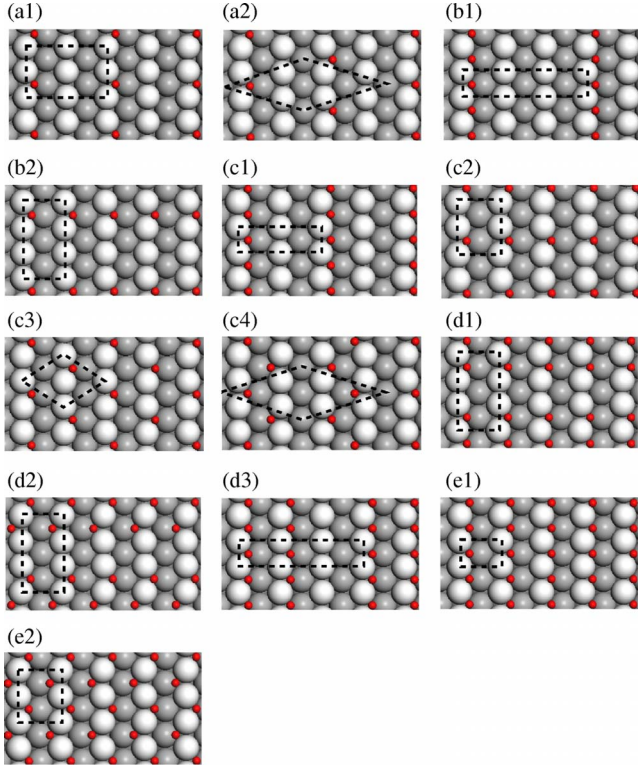
FIG. 3. (Color online) Top views on O/Re($10\bar{1}0$) for different coverages: (a1) (2×2)-1O and (a2) $c(2\times4)$-1O at 0.25 GML; (b1) (1×3)-1O and (b2) (3×1)-1O at 0.33 GML; (c1) (1×2)-1O, (c2) (2×1)-1O, (c3) $c(2\times2)$-1O, and (c4) $c(2\times4)$-2O at 0.50 GML; (d1) (3×1)a-2O, (d2) (3×1)b-2O, and (d3) (1×3)-2O at 0.66 GML; (e1) (1×1)-1O and (e2) $(2\times1)p2mg$-2O at 1.00 GML.

TABLE III. Binding energies for oxygen adsorbed at three-fold hollow H1-sites of unreconstructed Re($10\bar{1}0$)-(1×1) with different overlayers and coverages.

Structure	Coverage (GML)	E_{bind} (eV)
(2×2)-1O [Fig. 3(a1)]	0.25	3.76
$c(2\times4)$-1O [Fig. 3(a2)]	0.25	3.75
(1×3)-1O [Fig. 3(b1)]	0.33	3.59
(3×1)-1O [Fig. 3(b2)]	0.33	3.66
(2×1)-1O [Fig. 3(c1)]	0.50	3.73
(1×2)-1O [Fig. 3(c2)]	0.50	3.60
$c(2\times2)$-1O [Fig. 3(c3)]	0.50	3.77
$c(2\times4)$-2O [Fig. 3(c4)]	0.50	3.79
(1×3)-2O [Fig. 3(d1)]	0.66	3.60
(3×1)a-2O [Fig. 3(d2)]	0.66	3.61
(3×1)b-2O [Fig. 3(d3)]	0.66	3.57
(1×1)-1O [Fig. 3(e1)]	1.00	3.60
$(2\times1)p2mg$-2O [Fig. 3(e2)]	1.00	3.41
(1×3)-4O [Fig. 4(a)]	1.33	3.28
(1×2)-3O [Fig. 4(b)]	1.50	3.17
(1×3)-5O [Fig. 4(c)]	1.66	3.01
(1×1)-2O [Fig. 4(d)]	2.00	2.76

with a binding energy of 3.66 eV, is 0.07 eV more stable than the former. This preference might be explained by (i) the weaker O-O repulsion along each substrate row or (ii) the tendency of O atoms to not share Re atoms along each substrate row.

Among the different adsorbate structures possible with 0.50 GML, we studied: (1×2)-1O, (2×1)-1O, $c(2\times2)$-1O, and $c(2\times4)$-2O. Top views of these configurations are shown in Figs. 3(c1)–3(c4). The $c(2\times4)$-2O structure is found to be most stable, having an average binding energy per oxygen of 3.79 eV. This is in good agreement with the results obtained by other groups for the O/Co($10\bar{1}0$) (experiment)[39] and O/Ru($10\bar{1}0$) (theory and experiment)[11] systems. Oxygen adsorption on Co($10\bar{1}0$) at low coverages leads to a metastable $c(2\times4)$-2O phase, which forms a (2×1)-1O upon heating. LEED experiments and DFT calculations on Ru($10\bar{1}0$) also showed the existence of a $c(2\times4)$-2O adlayer. It seems that with 0.50 GML the interaction between oxygen and Re($10\bar{1}0$) is significantly stronger than that between oxygen and Ru($10\bar{1}0$) (Ref. 11) by 0.98 eV.

For 0.66 GML we modeled (1×3)-2O and (3×1)-2O overlayers as shown in Figs. 3(d1)–3(d3). With the (3×1) surface unit cell, two different structures were considered, namely (3×1)a- and (3×1)b-2O. It was found that the

(3×1)a-2O configuration $(E_{bind}=3.61$ eV) is more stable. Since the difference between the binding energies of (1×3)-2O, proposed by experiments, and (3×1)a-2O is very small, this suggests that both structures might be possible (or coexist) on the surface.

At a coverage of 1.00 GML, we considered the (1×1)-1O and $(2\times1)p2mg$-2O structures as shown in Figs. 3(e1) and 3(e2). Our calculations indicate that the former is more stable by 0.19 eV. The calculated binding energy of 3.60 eV for (1×1)-1O is similar to the value obtained for the (1×2)-1O, (1×3)-1O, and (1×3)-2O adlayers, showing minor impact of interactions between adatoms bound to adjacent rows.
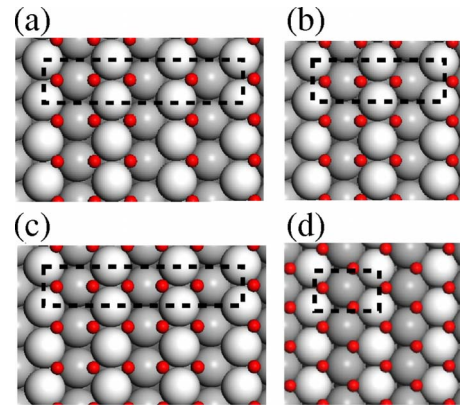
FIG. 4. (Color online) Top views on O/Re($10\bar{1}0$) with coverages >1.00 GML: (a) (1×3)-4O with 1.33 GML; (b) (1×2)-3O with 1.50 GML; (c) (1×3)-5O with 1.66 GML; (d) (1×1)-2O with 2.00 GML.
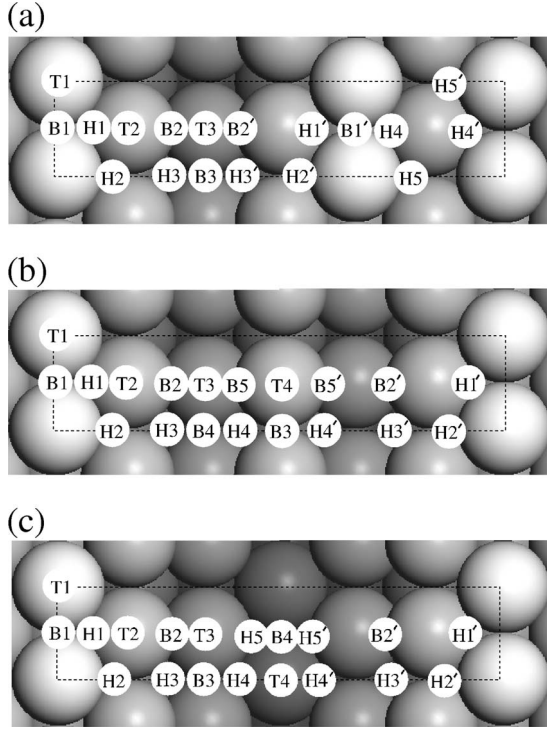
FIG. 5. Top views of (a) Re(10$\bar{1}$0)-(1×3) single MR, (b) Re(10$\bar{1}$0)-(1×3) double-MR, and (c) Re(10$\bar{1}$0)-(1×3) triple-MR, showing all binding sites at which O adsorption has been studied.

For coverages above 1.00 GML, first we focused on structures with two O atoms per unit cell (θ=2.00 GML) to obtain more knowledge about the interactions between adsorbates. This information was then used to predict stable adlayer configurations for the following coverages: 1.33 [(1×3)-4O], 1.50 [(1×2)-3O], and 1.66 GML [(1×3)-5O]. At 2.00 GML, a variety of adsorbate overlayers could form. Using the position labeling of Fig. 2, several possible combinations of distinguishable surface sites have been studied. Among these configurations occupying threefold hollow H1- and H2-sites [Fig. 4(d)] leads to the highest adsorption energy of 2.76 eV. Afterwards, we investigated the most probable configurations for 1.33, 1.50, and 1.66 GML shown in Fig. 4(a)–4(c). It turned out that structures in which all adsorbates occupy H1-sites [Figs. 4(a1), 4(b1), and 4(d1)] are energetically more favorable than those with adatoms at H2-sites [Figs. 4(a), 4(b2), and 4(c2)].

2. Reconstructed O/Re(10$\bar{1}$0)-(1×2) and O/Re(10$\bar{1}$0)-(1×3)

For O on reconstructed Re(10$\bar{1}$0) surfaces, we studied oxygen binding at several possible adsorption sites shown in
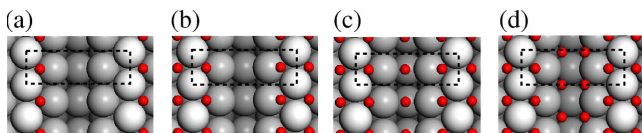
FIG. 6. (Color online) Top views of the most stable O/Re(10$\bar{1}$1)-(1×2) structures for different coverages: (a) 0.50, (b) 1.00, (c) 1.50, (d) 2.00 GML.
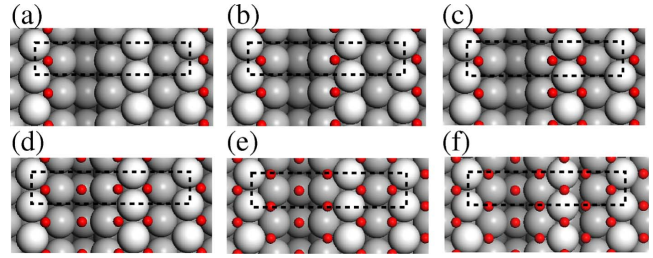
FIG. 7. (Color online) Top views of the most stable O/Re(10$\bar{1}$1)-(1×3) single-MR structures for different coverages: (a) 0.33, (b) 0.66, (c) 1.00, (d) 1.33, (e) 1.66, (f) 2.00 GML.

Fig. 5 for the single, double, and triple-MR surface structures that were described in Sect. II. The Re(10$\bar{1}$0)-(1×3) single-MR shown in Fig. 5(a) can be viewed as a combination of the unreconstructed Re(10$\bar{1}$0)-(1×1) and the Re(10$\bar{1}$0)-(1×2) surfaces. This allowed us to reduce the computational effort for reconstructed Re(10$\bar{1}$0)-(1×2) by studying only the most favorable arrangements of oxygen atoms in the (1×2) part of the Re(10$\bar{1}$0)-(1×3) single-MR surface. By this approach we additionally reduced possible numerical uncertainties related to switching the surface model.

As with the unreconstructed surfaces discussed in the previous section, we started our studies with one O per unit cell, finding again threefold hollow H1 sites to be most stable for all the considered reconstructed surfaces. While the calculated binding energies at H1-sites are very similar for single-MR (E_{bind}=3.81 eV), double-MR (E_{bind}=3.84 eV), and triple-MR (E_{bind}=3.83 eV) reconstructions on Re(10$\bar{1}$0)-(1×3), a slightly stronger binding (E_{bind}=3.89 eV) is obtained on Re(10$\bar{1}$0)-(1×2). Interestingly, the energy differences between different sites on each of the reconstructed surfaces are much smaller than those on Re(10$\bar{1}$0)-(1×1) for low coverages.

In order to explore the preferred overlayers with more than one O adatom per surface unit cell, we considered several possible combinations of distinguishable surface sites (as labeled in Fig. 5). Figures 6–9 summarize the most favorable structures obtained for different oxygen coverages on Re(10$\bar{1}$0)-(1×2) and Re(10$\bar{1}$0)-(1×3) surfaces. The corresponding binding energies as function of surface coverage are plotted in Fig. 10 and listed in Tables IV and V. In Fig.
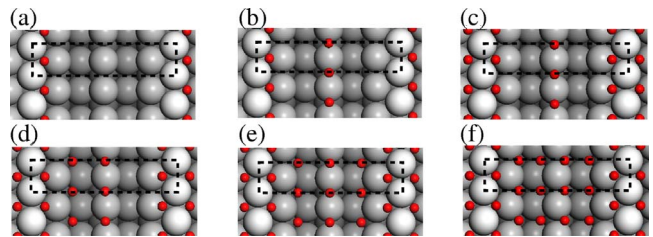
FIG. 8. (Color online) Top views of the most stable O/Re(10$\bar{1}$1)-(1×3) double-MR structures for different coverages: (a) 0.33, (b) 0.66, (c) 1.00, (d) 1.33, (e) 1.66, (f) 2.00 GML.
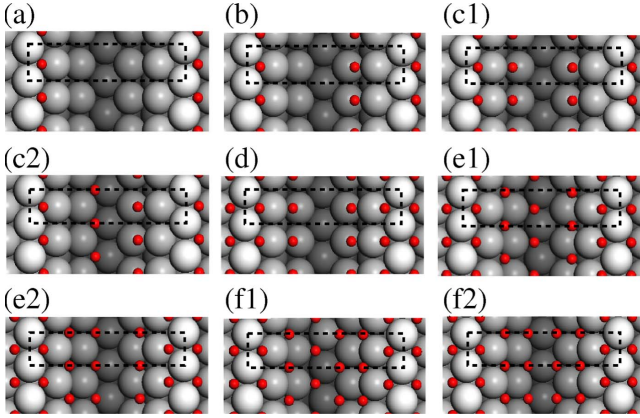
FIG. 9. (Color online) Top views of the most stable O/Re(10$\bar{1}$1)-(1×3) triple-MR structures for different coverages: (a) 0.33, (b) 0.66, (c1 and c2) 1.00, (d) 1.33, (e1 and e2) 1.66, (f1 and f2) 2.00 GML.

10 we also include the results obtained for unreconstructed O/Re(10$\bar{1}$0)-(1×1). While at higher coverages the curves are relatively smooth, some discontinuities appear for coverages lower than 1.00 GML on the unreconstructed surface. This is related to the existence of a pronounced *row pairing* of Re atoms (see Ref. 40 for details), which causes the binding energies to increase by ∼0.1 eV at 0.25 and 0.50 GML. Interestingly, Fig. 10 indicates that the adsorption energy of O is higher on the reconstructed surfaces than on Re(10$\bar{1}$0)-(1×1) for most of the considered coverages (except at 1.00 GML). Apparently, the stabilization resulting from the missing-row reconstruction is more significant at higher coverages, indicating that additional O atoms prefer positions in the troughs of the missing rows. Therefore, at the highest coverage examined (2.00 GML), the strongest binding energy is obtained on the triple-MR structure that has the deepest trough among the studied systems.

D. Surface phase diagram of O/Re(10$\bar{1}$0)

The energies obtained for all clean and oxygen covered surfaces discussed in the previous two sections have then
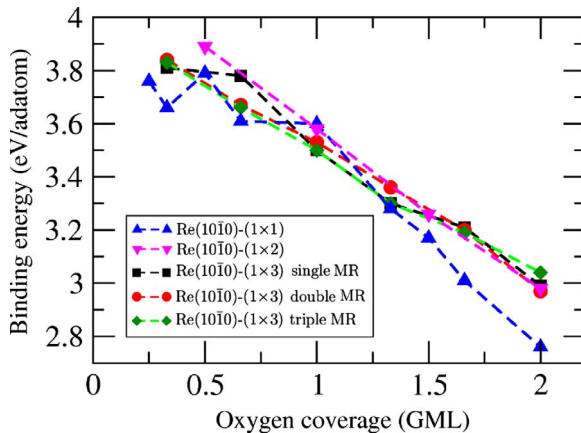
FIG. 10. (Color online) Binding energy (referenced to $\frac{1}{2}O_2$) as a function of oxygen coverage on Re(10$\bar{1}$0).

TABLE IV. Binding energies (referenced to $\frac{1}{2}O_2$) for oxygen on the reconstructed Re(10$\bar{1}$0)-(1×2) surface at different coverages; only the most stable structure for each coverage is listed.

Coverage (GML)	E_{bind} (eV)
0.50 [Fig. 6(a)]	3.89
1.00 [Fig. 6(b)]	3.58
1.50 [Fig. 6(c)]	3.26
2.00 [Fig. 6(d)]	2.98

been used to generate a surface phase diagram using Eq. (7) with the theoretically obtained surface areas.[41] Figure 11 shows the resulting surface phase diagram, where the surface free energy γ is plotted versus the chemical potential of the surrounding oxygen referenced by $\Delta\mu_O = \mu_O - 1/2E_{O_2}^{\text{tot}}$. Since our focus is on oxygen adsorption on pure Re, the phase diagram is valid in the oxygen chemical potential range, where the bulk oxide is not stable. We calculated the heat of formation of ReO$_2$ to be −2.24 eV per oxygen and shaded the $\Delta\mu_O \geq −2.24$ eV range in the phase diagram.

The phase diagram indicates that at oxygen chemical potentials $\Delta\mu_O < −3.67$ eV all oxygen should be desorbed and, therefore, the unreconstructed Re(10$\bar{1}$0)-(1×1) orientation is thermodynamically preferred. Increasing the oxygen chemical potential results in the formation of a $c(2×4)$-2O overlayer on unreconstructed Re(10$\bar{1}$0)-(1×1) [see Fig. 12(b)] between $\Delta\mu_O = −3.67$ and −3.56 eV. Further increase up to −1.85 eV only leads to an increase in the adsorbate coverage [see Figs. 12(c) and 12]. Interestingly, for $\Delta\mu_O \geq −1.85$ eV, the (1×3)-6O overlayer on the reconstructed Re(10$\bar{1}$0)-(1×3) triple-MR surface [see Figs. 12(e) and 12(e′)] becomes stable. Finally, from the thermodynamic viewpoint ReO$_2$ bulk-oxide should form at oxygen chemical potentials above −2.24 eV. However, the formation of the corresponding bulk oxide might be kinetically hindered, which could result in metastable adlayer structures even at $\Delta\mu_O > −2.24$ eV.[42]

TABLE V. Binding energies (referenced to $\frac{1}{2}O_2$) for oxygen on the reconstructed Re(10$\bar{1}$0)-(1×3) surfaces at different coverages; only the most stable structure for each coverage is listed.

Coverage (GML)	Single-MR E_{bind} (eV)	Double-MR E_{bind} (eV)	Triple-MR E_{bind} (eV)
0.33	3.81 [Fig. 7(a)]	3.84 [Fig. 8(a)]	3.83 [Fig. 9(a)]
0.66	3.78 [Fig. 7(b)]	3.67 [Fig. 8(b)]	3.66 [Fig. 9(b)]
1.00	3.50 [Fig. 7(c)]	3.53 [Fig. 8(c)]	3.50 [Fig. 9(c1)]
			3.50 [Fig. 9(c2)]
1.33	3.30 [Fig. 7(d)]	3.36 [Fig. 8(d)]	3.30 [Fig. 9(d)]
1.66	3.21 [Fig. 7(e)]	3.20 [Fig. 8(e)]	3.19 [Fig. 9(e1)]
			3.19 [Fig. 9(e2)]
2.00	2.99 [Fig. 7(f)]	2.97 [Fig. 8(f)]	3.04 [Fig. 9(f1)]
			3.04 [Fig. 9(f2)]
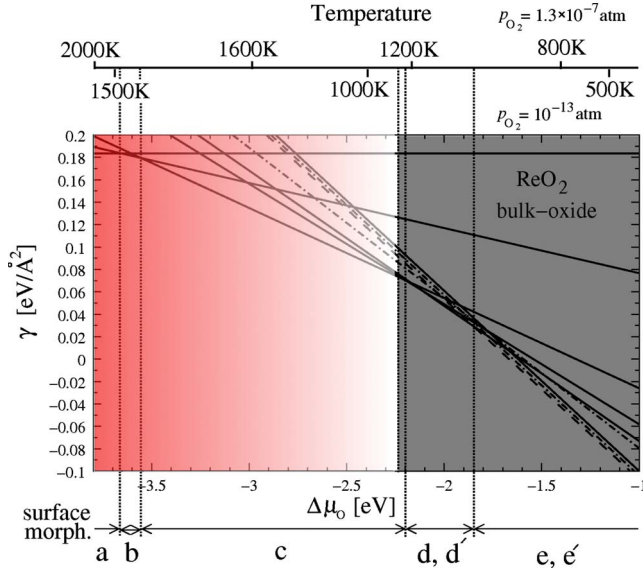
FIG. 11. (Color online) Surface phase diagram for O adsorption on Re($10\bar{1}0$), showing the surface free energy as function of the oxygen chemical potential referenced as $\Delta\mu_O = \mu_O - \frac{1}{2}E_{O_2}^{tot}$. Labels a–e′ refer to the surface structures shown in Fig. 12.

In order to allow for a better comparison with the different experiments, the oxygen chemical potential has been converted to temperature scales for oxygen partial pressures of 1.3×10^{-7} and 1.0×10^{-13} atm as used experimentally by Zehner et al.[14] and Lenz et al.,[15] respectively (see upper scales in Fig. 11). It can be seen that at an oxygen partial pressure of 1.3×10^{-7} atm (10^{-13} atm) no oxygen is adsorbed on the surface for $T \geq 1950$ K ($T \geq 1500$ K). This high-desorption temperature is directly related to the rather strong binding energy of oxygen to Re($10\bar{1}0$) (3.79 eV per $\frac{1}{2}O_2$). Since entropy contributions that have been neglected here might become relevant as temperature rises, at high temperatures only a qualitative understanding of the surfaces phases can be gained. To illustrate this limitation, the high temperature region of the phase diagram has been shaded red. Thus, the more quantitative analysis is restricted to the low-temperature phases.

At oxygen partial pressures of 1.3×10^{-7} atm and $T=1300$ K a (1×1) adlayer with 1.00 GML should form on unreconstructed Re($10\bar{1}0$)-(1×1) [Fig. 12(c)]. However, at

this temperature the stability differences to the (1×3)-4O and (1×2)-3O phases [Figs. 12(d) and 12(d′)] are rather small (5–8 meV/Å^2). Therefore, from our calculations all three adlayers could be possible, which would conform to the (1×3) adlayer observed by Zehner et al. (at the same environmental conditions). Figure 11 also shows that for 1220 K$\geq T \geq$ 1040 K there might be a coexistence of the (1×3)-4O and (1×2)-3O adlayers on still unreconstructed Re($10\bar{1}0$)-(1×1). Finally, at $T \leq 1040$ K, the oxygen coverage increases to 2.00 GML that leads to the reconstruction of the surface into the Re($10\bar{1}0$)-(1×3) triple-MR configuration as shown in Figs. 12(e) and 12(e′). Although without adsorbate the surface free energy of the triple-MR reconstructed surface was considerably larger than the unreconstructed surface, the strongly interacting oxygen finally increases the stability of the reconstructed surface (by ~ 8 meV/Å^2) at high coverages and finally induces the surface reconstruction.

As mentioned above, the triple-MR structures can be viewed as $\{10\bar{1}1\}$ microfacets on the ($10\bar{1}0$) surface. Interestingly, this kind of facet was proposed by Zehner et al. for temperatures of 888 K or higher and $p_{O_2}=1.3\times10^{-7}$ atm, without further determination of the facet sizes. Our calculations indicate that while infinitely large facets exhibiting $\{10\bar{1}1\}$ faces do not appear as stable phases, $\{10\bar{1}1\}$ microfacets that expose three Re layers could form [i.e., Re($10\bar{1}0$)-(1×3) triple MR]. Since we find that for $p_{O_2}=1.3\times10^{-7}$ atm the orthorhombic ReO$_2$ bulk oxide becomes thermodynamically stable already below 1240 K, the $\{10\bar{1}1\}$ facets observed experimentally at $T \geq 888$ K are most probably metastable structures that appear due to kinetic limitations in the formation of ReO$_2$ bulk oxide.

Compared to the experiments by Lenz et al.,[15] who have proposed a (1×3)-2O overlayer at $T<780$ K and $p_{O_2}=10^{-13}$ atm, our phase diagram reproduces the (1×3) periodicity but indicates two possible adlayer configurations with higher coverages. Furthermore, we could show that this periodicity resembles the reconstruction of the surface introduced by the adsorption of oxygen.

Finally, in order to investigate the sensitivity of our results on choosing a different exchange-correlation functional, we additionally calculated the most relevant surface structures with the LDA functional and generated the equivalent surface phase diagram. Figure 13 shows the stability range of

FIG. 12. (Color online) Surface structures for the stable O/Re($10\bar{1}0$) surface phases (see Fig. 11): (a) clean Re($10\bar{1}0$)-(1×1), (b) c(2×4)-2O overlayer on Re($10\bar{1}0$)-(1×1), (c) (1×1)-1O overlayer on Re($10\bar{1}0$)-(1×1), (d) (1×3)-4O overlayer on Re($10\bar{1}0$)-(1×1), (d′) (1×2)-3O overlayer on Re($10\bar{1}0$)-(1×1), (e) and (e′) (1×3)-6O overlayer on Re($10\bar{1}0$)-(1×3) triple MR.
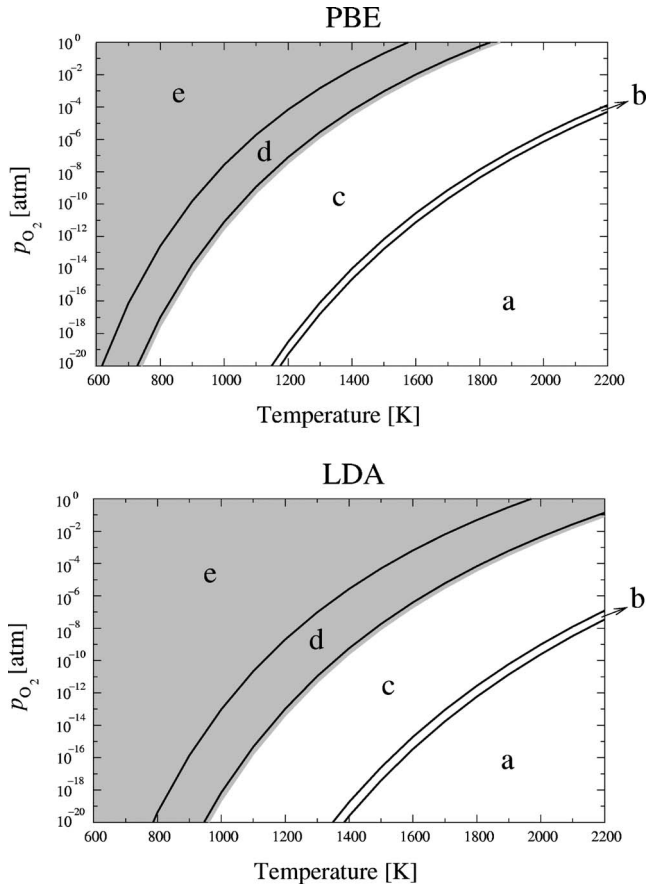
FIG. 13. Surface phase diagrams for the Re(10$\bar{1}$0) surface in contact with an O$_2$ gas phase for the PBE and LDA exchange-correlation functional. The structure-labeling corresponds to the models shown in Fig. 12.

different phases with respect to temperature and pressure evaluated using the PBE and LDA functional. It can be seen that although with the LDA functional all phase transitions are shifted toward higher temperatures (by 200–250 K), the overall phase ordering and therefore the conclusions drawn above remain unchanged.

IV. CONCLUSION

In this paper, we investigated clean and oxygen-covered surfaces of unreconstructed and reconstructed Re(10$\bar{1}$0) using density functional theory calculations in tandem with

TABLE VI. Comparison of the relative oxygen binding energies and surface free energies for 1.00 GML O adsorbed on Re(10$\bar{1}$0)-(1×1) using an all electron (AE) and a pseudopotential (PP) approach.

Method	ΔE_{bind} (eV)	$\Delta \gamma$ (meV/Å^2)
AE	1.584	127.4
PP	1.599	128.6
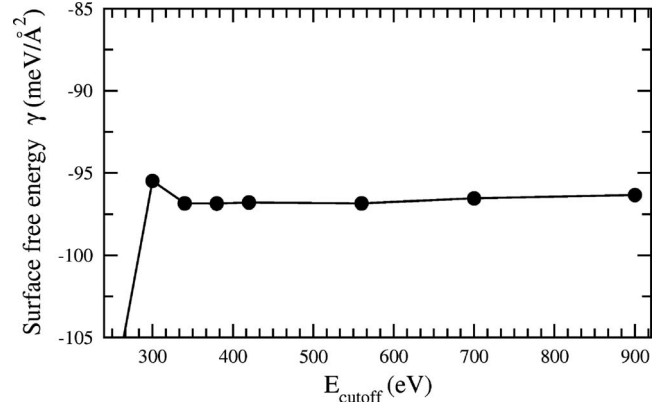
FIG. 14. The surface free energy γ as function of energy cutoff for O/Re(10$\bar{1}$0)-(1×1) with 1.00 GML coverage.

thermodynamic considerations, providing detailed information on the structure and energetics of a variety of oxygen coverages. It has been shown that on Re(10$\bar{1}$0) adsorption of atomic oxygen at coverages ≥2.00 GML leads to the stabilization of a (1×3) triple-MR reconstruction, being comparable to a nanofaceted surface exposing (10$\bar{1}$1) faces. Due to this morphological change of the surface, stable adlayer structures, that have been observed experimentally, follow the same (1×3) periodicity. As the oxygen adsorbate induces the surface reconstruction, our work has important implications for Re-based catalysts that operate under oxygen-rich conditions. While characterizations before or after any catalytic reaction will indicate an unreconstructed Re(10$\bar{1}$0) surface, under steady-state conditions the surface might actually be reconstructed.

ACKNOWLEDGMENTS
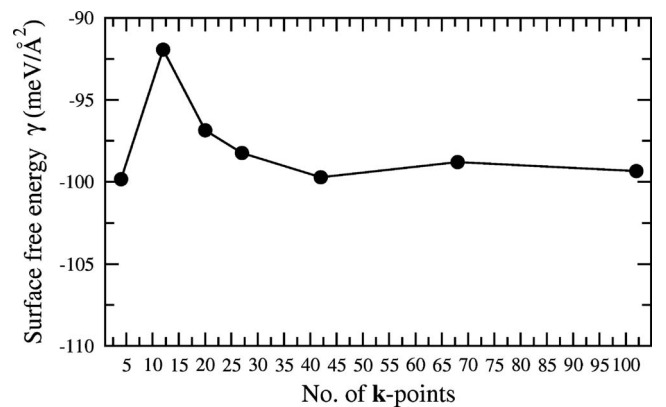
FIG. 15. The surface free energy γ as function of total number of **k** points for O/Re(10$\bar{1}$0)-(1×1) with 1.00 GML coverage.
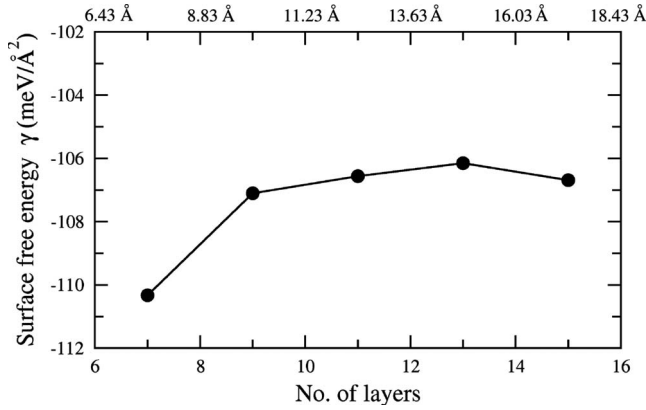
FIG. 16. The surface free energy γ as function of the number of layers (or slab thickness) for O/Re($10\bar{1}0$)-(1×1) with 1.00 GML coverage.

APPENDIX: ACCURACY OF THE SURFACE FREE ENERGY

Since our studies are based on a PP treatment of the core electrons, before studying the convergence of the different calculational parameters, we investigated the numerical uncertainties related to the use of pseudopotentials. To estimate these uncertainties we compared the relative binding energies for the adsorption of 1.00 GML oxygen at two different binding sites of Re($10\bar{1}0$)-(1×1) (sites B1 and T2, see Fig. 2) to a corresponding all electron calculation (for which we used the WIEN2K code with similar parameters[26]). Table VI shows the difference in the binding energies obtained with both methods, which finally leads to a difference in $\Delta\gamma$ of only ~1.2 meV/Å^2.

The accuracy of the results also depends on the plane wave cutoff, number of **k** points, slab thickness, and vacuum size. To find the optimum value for each parameter we independently evaluated the convergence behavior of the surface free energy for O/Re($10\bar{1}0$)-(1×1) and O/Re($10\bar{1}1$)-(1×1). All convergence calculations presented below were performed with the PBE functional, as the re-
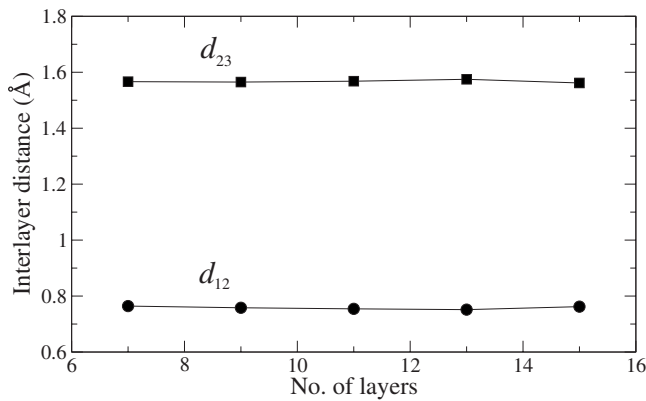
FIG. 17. The interlayer distance between the first and second layer (d_{12}) and the second and third layer (d_{23}) as a function of the number of layers (or slab thickness) for O/Re($10\bar{1}0$)-(1×1) with 1.00 GML coverage.
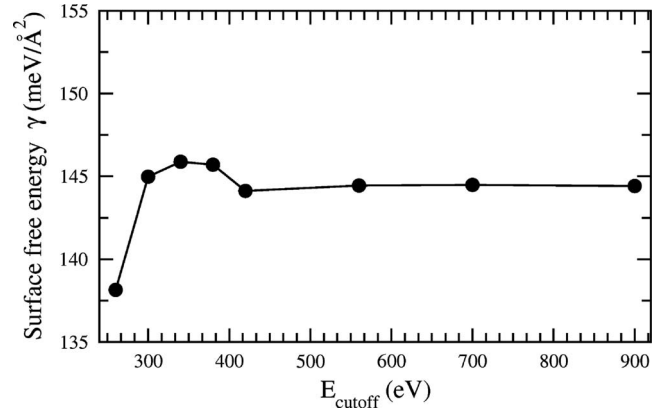
FIG. 18. The surface free energy γ as function of energy cutoff for O/Re($10\bar{1}1$)-(1×1) with 1.00 GML coverage.

sults discussed in the main paper are primarily based on these values. To minimize the number of influencing parameters, convergence tests related to the plane wave energy cutoff, number of **k** points, and vacuum size were based on fixed (preoptimized) geometries, while in our studies on the slab thickness the surface and adsorbates were allowed to freely relax (except the bottom four Re layers that were kept fixed at the calculated bulk positions). The error bars were determined by comparing the surface free energies for a particular value with that when using the highest considered parameter value.

1. Re($10\bar{1}0$)

The surface free energy was calculated for plane-wave energy cutoffs between 260 and 900 eV. Figure 14 shows that γ does not change significantly for $E_{cutoff} \geq 380$ eV. At this energy-cutoff γ is converged up to 1 meV/Å^2.

Using the converged value of $E_{cutoff}=380$ eV, we afterwards varied the total number of **k** points between 4 and 102, corresponding to 2×4 and 12×17 Monkhorst-Pack (MP) **k**-point meshes. As Fig. 15 indicates, convergence is reached with 20 **k** points or a 5×8 MP grid, leading to remaining variations in γ of <2.5 meV/Å^2.
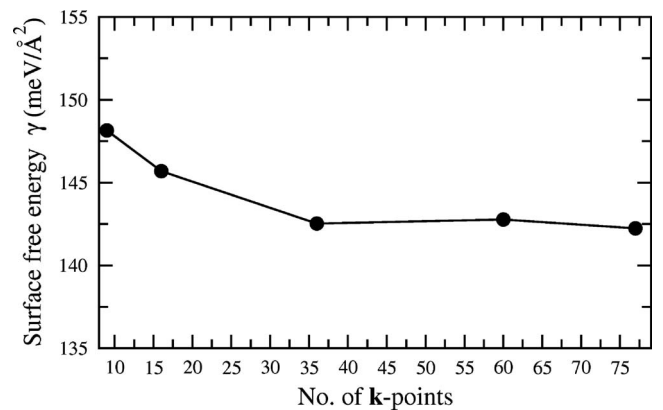
FIG. 19. The surface free energy γ as function of total number of **k** points for O/Re($10\bar{1}1$)-(1×1) with 1.00 GML coverage.
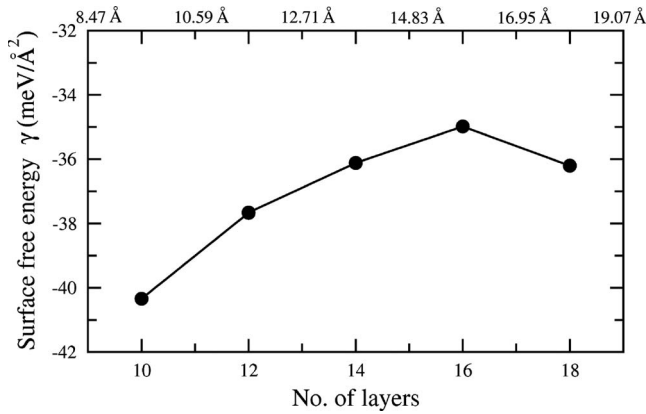
FIG. 20. The surface free energy γ as function of the number of layers (or slab thickness) for O/Re($10\bar{1}1$)-(1×1) with 1.00 GML coverage.

FIG. 21. The interlayer distance between the first and second layer (d_{12}) and the second and third layer (d_{23}) as a function of the number of layers (or slab thickness) for O/Re($10\bar{1}1$)-(1×1) with 1.00 GML coverage.

For the slab thickness, we varied the number of Re layers between 7 and 15 (thickness of 7.21 to 16.83 Å), leading to the behavior shown in Fig. 16. We find that slabs with 9 Re-layers (thickness of 10.03 Å) give satisfactory results, showing convergence up to 1 meV/Å^2. However, since for the reconstructed Re-surfaces atoms in the first and second layers are missing, we finally decided to model Re($10\bar{1}0$)-($1 \times n$), $n=1,2,3$ reconstructed surfaces with 11 layers.

Besides the surface free energies we also analyzed the surface relaxation behavior as function of the slab thickness of the unreconstructed surface (see Fig. 17). As one might have expected, the layer separations between the outermost layers (d_{12} and d_{23}) were found to be much less sensitive to the slab thickness, remaining almost constant for slabs of ≥ 8 layers.

Afterwards we checked the vacuum size, which was varied between 13 and 20 Å. Changes in the surface free energy were determined to be smaller than 0.5 meV/Å^2. Therefore, a vacuum size of 13 Å was found to be sufficiently large to separate periodically repeated slabs.

It should be mentioned that there is still an error source introduced by using different surface unit cells for Re($10\bar{1}0$)-($1 \times n$), $n=1,2,3$. This uncertainty was estimated by evaluating the binding of 1.00 GML oxygen on unreconstructed Re($10\bar{1}0$) with ($1 \times n$), $n=1,2,3$ unit cells. For the related surface free energies we found a variation of ~ 3 meV/Å^2, which is most likely due to the different **k**-point samplings. Finally, adding all these uncertainties leads to an upper limit of the overall error of ~ 8 meV/Å^2. We expect that uncertainties arising from these parameters should be even smaller when comparing different adsorption structures and coverages on the same surface (due to possible error cancellations).
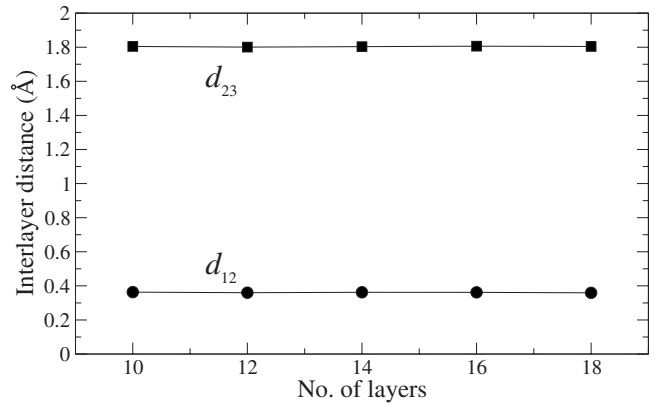
2. Re($10\bar{1}1$)

Performing the same convergence studies as discussed before for O/Re($10\bar{1}1$)-(1×1), we found (see Figs. 18–21) uncertainties in γ of 1.5, 3.5, 0.5, and 0.5 meV/Å^2 when using a plane wave energy cutoff of 380 eV, a total number of 16 **k** points (corresponding to a 4×8 mesh), a slab thickness of 14 layers, and a vacuum of ~ 13 Å. Again, summation of these uncertainties and the one related to the use of pseudopotentials (see above) leads to ~ 8 meV/Å^2.

*timo.jacob@uni-ulm.de

[1] A. V. Naumov, Russ. J. Non-Ferrous Metals **48**, 418 (2007).

[2] I. E. Wachs, G. Deo, A. Andreini, M. A. Vuurman, and M. de Boer, J. Catal. **160**, 322 (1996).

[3] Y. Z. Yuan, T. Shido, and Y. Iwasawa, Chem. Commun. (2000) 1421.

[4] J. Liu, E. Zhan, W. Cai, J. Li, and W. Shen, Catal. Lett. **120**, 274 (2008).

[5] M. E. Bussell, A. J. Gellman, and G. A. Somorjai, J. Catal. **110**, 423 (1988).

[6] M. Asscher, J. Carrazza, M. M. Khan, K. B. Lewis, and G. A. Somorjai, J. Catal. **98**, 277 (1986).

[7] R. Kojima, H. Enomoto, M. Muhler, and K. Aika, Appl. Catal.,

A **246**, 311 (2003).

[8] H. Wang, Ph.D. thesis, Rutgers University, 2008.

[9] M. Reyhan, H. Wang, and T. E. Madey, Catal. Lett. **129**, 46 (2009).

[10] T. E. Madey, W. Chen, H. Wang, P. Kaghazchi, and T. Jacob, Chem. Soc. Rev. **37**, 2310 (2008).

[11] S. Schwegmann, A. P. Seitsonen, V. De Renzi, H. Dietrich, H. Bludau, M. Gierer, H. Over, K. Jacobi, M. Scheffler, and G. Ertl, Phys. Rev. B **57**, 15487 (1998).

[12] H. L. Davis and D. M. Zehner, J. Vac. Sci. Technol. **17**, 190 (1980).

[13] D. Rosenthal, I. Zizak, N. Darowski, T. T. Magkoev, and K. Christmann, Surf. Sci. **600**, 2830 (2006).

[14] D. M. Zehner and H. E. Farnsworth, Surf. Sci. **30**, 335 (1972).

[15] J. Lenz, P. Rech, K. Christmann, M. Neuber, C. Zubragel, and E. Schwarz, Surf. Sci. **269-270**, 410 (1992).

[16] M. Gierer, H. Over, P. Rech, P. Schwarz, and K. Christmann, Surf. Sci. Lett. **370**, L201 (1997).

[17] E. Kaxiras, Y. Bar-Yam, J. D. Joannopoulos, and K. C. Pandey, Phys. Rev. B **35**, 9625 (1987).

[18] M. Scheffler, *Physics of Solid Surfaces* (Elsevier, Amsterdam, 1987).

[19] G.-X. Qian, R. M. Martin, and D. J. Chadi, Phys. Rev. B **38**, 7649 (1988).

[20] K. Reuter and M. Scheffler, Phys. Rev. B **65**, 035406 (2001).

[21] M. D. Segall, P. L. D. Lindan, M. J. Probert, C. J. Pickard, P. J. Hasnip, S. J. Clark, and M. C. Payne, J. Phys.: Condens. Matter **14**, 2717 (2002).

[22] D. Vanderbilt, Phys. Rev. B **41**, 7892 (1990).

[23] J. P. Perdew, K. Burke, and M. Ernzerhof, Phys. Rev. Lett. **77**, 3865 (1996).

[24] *JANAF Thermochemical Tables*, 2nd ed., edited by D. R. Stull and H. Prophet (U.S. National Bureau of Standards, U.S. EPO, Washinghton D.C., 1971).

[25] C. Kittel, *Introduction to Solid State Physics* (Wiley, New York, 1996).

[26] P. Blaha, K. Schwarz, G. K. H. Madsen, D. Kvasnicka, and J. Luitz, *WIEN2k, An Augmented Plane* Wave+Local *Orbitals Program For Calculating Crystal Properties* (Technical University Vienna, Austria, 2001).

[27] W. X. Li, C. Stampfl, and M. Scheffler, Phys. Rev. B **65**, 075407 (2002).

[28] M. Todorova, K. Reuter, and M. Scheffler, J. Phys. Chem. B **108**, 14477 (2004).

[29] M. V. Ganduglia-Pirovano and M. Scheffler, Phys. Rev. B **59**, 15533 (1999).

[30] A. Soon, M. Todorova, B. Delley, and C. Stampfl, Phys. Rev. B **73**, 165424 (2006).

[31] D. G. Fedak and N. A. Gjostein, Acta Metall. **15**, 827 (1967).

[32] H. P. Bonzel and R. Ku, J. Vac. Sci. Technol. **9**, 663 (1972).

[33] P. Fery, W. Moritz, and D. Wolf, Phys. Rev. B **38**, 7275 (1988).

[34] E. C. Sowa, M. A. Van Hove, and D. L. Adams, Surf. Sci. **199**, 174 (1988).

[35] P. Fenter and T. Gustafsson, Phys. Rev. B **38**, 10197 (1988).

[36] E. Vlieg, I. K. Robinson, and K. Kern, Surf. Sci. **233**, 248 (1990).

[37] U. Korte and G. Meyer-Ehmsen, Surf. Sci. **271**, 616 (1992).

[38] The surface free energy was projected onto the planar $Re(10\bar{1}0)$ surface using $\gamma_{10\bar{1}1}^{\text{proj.}} = \gamma_{10\bar{1}1}/\cos \vartheta_{10\bar{1}1}$ with a geometrically obtained tilt-angle of $\vartheta_{10\bar{1}1} = 31.75°$.

[39] E. Schwarz, K. H. Ernst, C. Gonser-Buntrock, M. Neuber, and K. Christmann, Vacuum **41**, 180 (1990).

[40] P. Kaghazchi, Ph.D. thesis, Freie University Berlin, 2009.

[41] Since unsymmetric slabs were used, where we concentrated on the top surface of the slab only, we always subtracted the surface free energy of the fixed surfaces at the bottom of the slabs.

[42] P. Kaghazchi, T. Jacob, H. Wang, W. Chen, and T. E. Madey, Phys. Rev. B **79**, 132107 (2009).